



11

Abstract

12 The electrical conductivity of gabbroic melt with four different water contents (i.e.
13 0, 2.59 wt%, 5.92 wt% and 8.32 wt%) was measured at temperatures of 873–1373 K
14 and pressures of 1.0–3.0 GPa using YJ–3000t multi–anvil high–pressure apparatus and
15 Solartron–1260 impedance spectroscopy analyzer. At a fixed water content of 2.59 wt%,
16 the electrical conductivity of the sample slightly decreased with increasing pressure at
17 the temperature range of 873–1373 K, and its corresponding activation energy and
18 activation volume were determined as 0.87 ± 0.04 eV and -1.98 ± 0.02 cm³ mole⁻¹,
19 respectively. Under the certain conditions of 873–1373 K and 1.0 GPa, the electrical
20 conductivity of the gabbroic melts tends to gradually increase as the rise of water
21 content from 0 to 8.32 wt%, and the activation enthalpy decreases from 0.93 eV to 0.63
22 eV, accordingly. Furthermore, the functional relation models for the electrical
23 conductivity of gabbroic melts with the variations of temperature, pressure and water
24 content were constructed at high–temperature and high–pressure conditions,
25 respectively. In addition, the dependence relation of the electrical conductivity of melts
26 with the degree of depolymerization was explored under conditions of four different
27 water contents, 1373 K and 1.0 GPa, and three previously available reported results on
28 those of representative calc–alkaline igneous rock melts (i.e. dacitic melt, basaltic melt
29 and andesitic melt) were detailedly compared. In comprehensive combination with our
30 presently acquired electrical conductivity data of gabbroic melt with four different
31 water contents and the available data of polycrystalline olivine, the electrical
32 conductivity of gabbroic melt–olivine system on the variation of volume percentage of



33 anhydrous and hydrous melts was successfully constructed by virtue of the typical
34 Hashin–Shtrikman upper bound model. In light of the electrical conductivity of
35 gabbroic melt–olivine system with the previous MT results, we find that the anhydrous
36 and hydrous gabbroic melts can be employed to reasonably interpret the high
37 conductivity anomalies in the Mohns ridge of the Arctic Ocean.

38 **Keywords: electrical conductivity, gabbroic melt, degree of depolymerization,**
39 **high conductivity anomalies, Mohns ridge**



40 **1 Introduction**

41 The hydrous melt for various rocks and minerals widely exists at active plate
42 tectonic boundaries such as mid-ocean ridge, subduction zone, orogenic belt, etc. (Shen
43 and Forsyth, 1995; White et al., 2001; Wallace, 2005; Wu et al., 2018; Sim et al., 2020;
44 Förster and Selway, 2021; Li et al., 2022; Turner and Langmuir, 2022). For the typical
45 Mohns ridge in the Arctic Ocean, there existed a large amount of high conductivity
46 anomaly phenomena with its correspondent magnitude of $0.08\text{--}0.32\text{ S m}^{-1}$ for the
47 gabbro-rich regions have been revealed on the basis of previous magnetotelluric (MT)
48 controlled source electromagnetic (CSEM) results (Johansen et al., 2019).

49 Previously available researches have indicated that gabbroic and basaltic melts
50 contain a large amount of water, and the water content for the certain type of melt may
51 be discrepant within the different depth ranges of the oceanic crust (Dixon et al., 1995;
52 Almeev et al., 2008; Shaw et al., 2010; Leuthold et al., 2018). Meanwhile, water content
53 is also considered as a crucial ingredient to possibly affect the electrical conductivity
54 of melt, and there are a large number of previously available reported results for the
55 variation of water content on the electrical conductivity of some representative calc-
56 alkaline igneous rock melts at high temperature and high pressure in the recently several
57 years (Ni et al., 2011; Laumonier et al., 2015; Guo et al., 2017; Chen et al., 2018). For
58 example, Ni et al. (2011) measured the electrical conductivity of hydrous basaltic melt
59 within water content range of 0–6.3 wt% at conditions of 1473–1923 K and 2.0 GPa,
60 and they found that the electrical conductivity of basaltic melt with a fixed water content
61 of 6.3 wt% was of the rough 1.0 order of magnitude higher than that of the anhydrous



62 sample. The electrical conductivity of dacitic melt within the water content range of 0–
63 12 wt% was systematically investigated by Laumonier et al. (2015) within temperature
64 range of 673–1623 K and pressures of 0.3–3.0 GPa. As pointed out by Laumonier et al.
65 (2015), the high conductivity anomalies in the Uturuncu Volcano could be explained
66 by the presence of hydrous dacitic melt. By virtue of a piston cylinder high–pressure
67 apparatus and sweeping–frequency impedance spectroscopy, Guo et al. (2017) obtained
68 the electrical conductivity data of andesitic melt within the water content range of 0.01–
69 5.90 wt% at conditions of 1164–1573 K and 0.5–1.0 GPa. Their experimental results
70 indicated that the presence of less than 20 vol% of hydrous andesitic melt within the
71 water content range of 6–9 wt% can be used to interpret the high conductivity anomalies
72 beneath the surface of the Uturuncu Volcano. Electrical conductivity measurements of
73 the hydrous leucogranitic melt by Chen et al. (2018) at conditions of 739–1680 K and
74 0.36–2.52 GPa were systematically carried out within the water content range of 2.73–
75 11.97 wt%. In comprehensive combination with previous magnetotelluric data in the
76 northwest Himalaya, they considered that water–rich leucogranitic melts with a volume
77 percentage range of 4–16 vol% can be applied to reasonably explain the high
78 conductivity anomalies in these regions.

79 For the natural gabbroic rock, some previously available electrical conductivity
80 results were obtained using the piston–cylinder and multi–anvil high–pressure
81 apparatus at high temperature and high pressure. Sato and Ida (1984) measured the
82 electrical conductivity of the olivine–gabbro containing gabbroic melt at the
83 temperature range from 1123 K to 1473 K and atmospheric pressure, and the effects of



84 ionic diffusion of charge carriers (i.e. sodium, iron, magnesium and/or calcium ions)
85 and geometric structure of melt on the electrical conductivity of olivine–gabbro samples
86 were detailedly explored. The measurements of electrical conductivity for natural
87 gabbro were carried out at conditions of 1023–1423 K and room pressure by Schilling
88 et al. (1997), and they proposed that the electrical conductivity of samples can be
89 enhanced by the increasing volume percentage of gabbroic melt. As for the natural
90 Oman gabbro, the electrical conductivity of gabbroic melt with the volume percentage
91 proportion of 34 % was ~1.0–2.0 orders of magnitude higher than that of melt–free
92 sample within the temperature range from 1073 K to 1523 K and pressures of 0.3–1.0
93 GPa (Maumus et al., 2005). However, the influence of water content on the electrical
94 conductivity of gabbroic melt at high temperature and high pressure was not
95 investigated in detail. Consequently, it is crucial to make a systematic investigation on
96 the electrical conductivity of gabbroic melt with different water contents at high–
97 temperature and high–pressure conditions.

98 In the present studies, a series of electrical conductivity on the gabbroic melts were
99 systematically performed under conditions of 873–1373 K, 1.0–3.0 GPa and the
100 variation of water content range from 0 to 8.32 wt%. The effects of temperature,
101 pressure and water content on the electrical conductivity of gabbroic melt are deeply
102 explored, and the functional relation models have been successfully established at high–
103 temperature and high–pressure conditions. In conjunction with the degree of
104 depolymerization, the electrical conductivity of gabbroic melt with different water
105 contents is compared with that of three representative calc–alkaline igneous rock melts



106 (i.e. dacitic melt, andesitic melt and basaltic melt). Based on the calculated electrical
107 conductivity of gabbroic melt–olivine system, its potential geophysical implication was
108 detailedly discussed in the Mohns ridge of the Arctic Ocean.

109 **2 Experimental procedures**

110 **2.1 Sample Preparation**

111 The natural gabbroic rock used in this study was collected from the ophiolite suite
112 in the region of Ganzi Tibetan autonomous prefecture, Sichuan province, China. By
113 virtue of the high–temperature quenched melt for the natural rock powder, the
114 anhydrous and hydrous gabbroic melts are successfully obtained. Firstly, the fresh
115 natural gabbro was finely crushed and ground into the sample powder with the grain
116 size of less than 50 μm in an agate mortar. Then, the sample powder was kept in the
117 furnace at 473 K to remove the absorbed water. To obtain the homogeneously initial
118 materials for the subsequent electrical conductivity measurement, the powder of
119 gabbroic rock was melted at the temperature of 1473 K for 1.5 hours and rapidly
120 quenched in a high–temperature muffle furnace. Further, gabbroic melt was crushed
121 and ground again into powder with a grain size less than 50 μm and stored in a vacuum
122 dry furnace at 373 K. To synthesize the hydrous gabbroic melt, the desired amount of
123 deionized water was added to the powder, and subsequently, the sample encapsulated
124 in a gold tube using the Lampert–Puk precise welding device. After that, the starting
125 hydrous gabbroic melts with different water contents were synthesized at conditions of
126 1373 K and 1.0–3.0 GPa for 12 hours in the YJ–3000t multi–anvil high–pressure
127 apparatus, and all of these obtained samples are homogeneous without any available



128 crystals or bubbles. Detailed hot-pressed sintering assemblage was similar to that
129 previously described by Hu et al. (2022a). Lastly, all of the gabbroic melts were
130 polished into cylinders with diameters of ~4.0–5.0 mm and heights of ~4.0–6.0 mm,
131 and kept in muffle furnace at 423 K for 10 hours to eliminate the absorbed water for
132 subsequent electrical conductivity measurements. The chemical compositions of
133 anhydrous and hydrous gabbroic melts were analyzed by virtue of the electronic probe
134 microscopy analysis (EPMA) at the State Key Laboratory of Ore Deposit Geochemistry,
135 Institute of Geochemistry, Chinese Academy of Sciences, Guiyang, China, as shown in
136 Table 1.

137 **2.2 High-pressure cell and impedance measurements**

138 High-pressure complex impedance measurements for gabbroic melt were
139 performed by using Solartron-1260 impedance spectroscopy analyzer in the YJ-3000t
140 multi-anvil high-pressure apparatus. The cross-section diagram of sample assembly
141 for electrical conductivity measurements was shown in Fig. 1. Before high-pressure
142 cell was assembled, the cubic pressure medium of pyrophyllite with dimension of
143 $32.5 \times 32.5 \times 32.5 \text{ mm}^3$ and insulation sleeves were baked at 1073 K in a muffle furnace
144 for 5 hours to remove the absorbed water. The sample was placed at the middle of the
145 alumina and magnesia insulation sleeves, and sandwiched with two symmetric nickel
146 electrodes. The electrode was connected with a $\text{Ni}_{97}\text{Al}_3$ wire to a Solartron-1260
147 impedance spectroscopy analyzer. To shield against external electromagnetism and
148 spurious signal interference, the nickel foil with a thickness of 0.025 mm was installed
149 between the alumina and magnesia sleeves, and linked to the Earth line. Three-layer



150 stainless steel sheets with a total thickness of 0.5 mm were adopted as the heater, which
151 were installed between the cubic pressure medium of pyrophyllite and alumina sleeve.
152 After that, the sample assembly was stored in the vacuum dry furnace at 423 K for at
153 least 12 hours before the electrical conductivity measurements.

154 During the experiment, the pressure was slowly raised with a rate of 1.0 GPa h^{-1}
155 until it reached the desired value, and then the temperature was gradually increased with
156 a speed of 5.0 K min^{-1} . Under predesignated high-temperature and high-pressure
157 condition, impedance spectra of samples were collected in the frequency range of 10^0 –
158 10^6 Hz and the applied signal voltage of 1.0 V. To obtain reproducible data, impedance
159 spectra of samples were measured at least two continuously heating-cooling cycles
160 under conditions of 873–1373 K and 1.0–3.0 GPa. The uncertainties of temperature and
161 pressure were less than 5.0 K and 0.1 GPa, respectively. The detailed experimental
162 principles and measurement procedures were described by Dai et al. (2008, 2009) and
163 Hu et al. (2022b).

164 **2.3 Determination of the water content**

165 The water content of gabbroic melt before and after the electrical conductivity
166 measurements was performed by virtue of the Vertex-70V and Hyperion-1000 vacuum
167 Fourier transform infrared (FT-IR) spectroscopy analyzer. The samples were double-
168 polished up to a thickness of $\sim 50 \text{ }\mu\text{m}$. At least five spectra were conducted on the
169 different regions of transparent sample surfaces and made an average value in order to
170 avoid the heterogeneity effect of water distribution. A detailed experimental method
171 and procedure for the FT-IR measurement was detailedly presented by Hong et al.



172 (2022) and Hu et al. (2022b). For the hydrous gabbroic melts, the signal of the
173 fundamental stretching H₂O vibrational spectroscopy at the peak position of ~3530
174 cm⁻¹ revealed to be oversaturated, which was similar to the previously obtained results
175 on hydrous dacitic melts reported by Laumonier et al. (2015). Two obviously
176 characteristic peaks were appeared at two correspondent wavenumbers of ~4500 cm⁻¹
177 and ~5200 cm⁻¹, which were representing the hydroxyl band and molecular water band
178 of gabbroic melts, respectively (Stolper, 1982; Dixon et al., 1995). Hence, the peak area
179 for the hydroxyl band and molecular water band was integrated to determine the water
180 content of sample. The typical FT-IR spectra of gabbroic melt within the wavenumbers
181 range of 2500–5800 cm⁻¹ are shown in Fig. 2. The water content of gabbroic melt (C_{melt})
182 can be worked out by Beer–Lambert law,

$$183 \quad C = \omega A / \epsilon \rho d \quad (1)$$

$$184 \quad C_{\text{melt}} = C_{\text{OH}} + C_{\text{H}_2\text{O}} \quad (2)$$

185 In here, the signal of ω stands for the molar mass of H₂O (18.02 g mole⁻¹), A stands for
186 the integrated area of absorption spectra (cm⁻²), ρ stands for the density (g cm⁻³), d
187 stands for the thickness of thin section (cm), and ϵ stands for the integral molar
188 absorption coefficient (L mole⁻¹·cm⁻²). As presented the calculated melt density method
189 by Luhr (2001), our density of gabbroic melt is determined as 2.764×10³ g L⁻¹. Molar
190 absorption coefficients of ϵ_{OH} and $\epsilon_{\text{H}_2\text{O}}$ were adopted from Dixon et al. (1995).
191 According to the Eqs. 1 and 2, the water contents for three obtained hydrous gabbroic
192 melts were calculated as 2.59 wt%, 5.92 wt% and 8.32 wt%, respectively. As displayed
193 in Table 2, there is no significant loss of water for hydrous gabbroic melt during the



194 electrical conductivity experiment.

195 **3 RESULTS**

196 In the present experiments, the electrical conductivity of gabbroic melt with four
197 different water contents (i.e. 0, 2.59 wt%, 5.92 wt% and 8.32 wt%) was measured at
198 temperature range of 873–1373 K and pressures of 1.0–3.0 GPa. The representative
199 complex impedance spectra of gabbroic melt with the 2.59 wt% water at conditions of
200 873–1373 K and 2.0 GPa were shown in Fig. 3. According to the theory of AC complex
201 impedance spectra (Huebner and Dillenburg, 1995; Xu, et al., 2000; Saltas et al., 2013,
202 2020; Dai and Karato, 2014, 2020), our acquired semicircular arc and additional tiny
203 tail represented the electrical transport process of grain interior and polarization process
204 at sample–electrode interface within the temperature range of 873–1123 K, respectively.
205 And thus, a series connection of R_S – CPE_S (R_S and CPE_S represent the resistance and
206 constant–phase element of the gabbroic melt, respectively) and R_E – CPE_E (R_E and CPE_E
207 represent the interface resistance and constant–phase element for electrode effect,
208 respectively) were employed as the equivalent circuit within a relatively lower
209 temperature range of 873–1123 K. As far as the higher temperature ranges of 1173–
210 1373 K, the equivalent circuit was consisted of the series connection of one resistance
211 and one parallel resistance with the constant phase element (CPE). The electrical
212 conductivity of sample can be calculated,

$$213 \quad \sigma = L/SR \quad (3)$$

214 In here, L , S and R stand for the length of sample (m), the cross–section area of electrode
215 (m^2) and the electrical resistance of sample (Ω), respectively. And the electrical



216 conductivity of gabbroic melt and temperatures conformed to the Arrhenius relation,

$$217 \quad \sigma = \sigma_0 \exp(-\Delta H/kT) \quad (4)$$

218 In here, σ_0 stands for the pre-exponential factor (S m^{-1}), k stands for the Boltzmann
219 constant (eV K^{-1}), and T stands for the absolute temperature (K), respectively. All of
220 these fitted parameters for the electrical conductivity of anhydrous and hydrous
221 gabbroic melt under conditions of 873–1373 K and 1.0–3.0 GPa were listed in Table 2.

222 For the gabbroic melt with a fixed water content of 2.59 wt%, the electrical
223 conductivity results for two continuously heating-cooling cycles at 873–1373 K and
224 3.0 GPa were shown in Fig. 4. In the first heating cycle within the temperature range of
225 923–1073 K, the electrical conductivity of sample was slightly deviated with those of
226 subsequent results in the first cooling and second heating-cooling cycles. Whereas, the
227 deviation degree became more and more small and finally overlapped at much higher
228 temperature range of 1123–1373 K. As a whole, the electrical conductivity of sample
229 was almost reproducible in the first cooling and second heating-cooling cycles. And
230 therefore, the electrical conductivity results were acquired by virtue of fitting
231 experimental data during the process of the first cooling and second heating-cooling
232 cycles.

233 **4 Discussions**

234 **4.1 Influence of pressure on electrical conductivity**

235 To identify the effect of pressure on the electrical conductivity of sample, the
236 electrical conductivity of hydrous gabbroic melt was acquired under condition of 873–
237 1373 K, 1.0–3.0 GPa and a fixed water content of 2.59 wt%. As illustrated in Fig. 5,



238 the electrical conductivity of sample and temperature conformed to the Arrhenius
239 relation at a certain water content and pressure condition. In the present studies, a
240 slightly negative dependence relation for the electrical conductivity of hydrous
241 gabbroic melt with a fixed water content of 2.59 wt% on the pressure was observed.
242 The electrical conductivity of sample slightly decreases by around 1.6 times at as
243 pressure enhances from 1.0 GPa to 3.0 GPa at temperature range of 873–1373 K.
244 Accordingly, the pre-exponential factor reduces from $3.02 \times 10^3 \text{ S m}^{-1}$ to $6.17 \times 10^2 \text{ S m}^{-1}$,
245 and the activation enthalpy value decreases from 0.85 eV to 0.81 eV, respectively.

246 Furthermore, the influence of pressure on the electrical conductivity of gabbroic
247 melt can be depicted as,

$$248 \quad \sigma = A_0(1-BP) \cdot \exp\left[-\frac{\Delta U + P\Delta V}{kT}\right] \quad (5)$$

249 In here, the pre-exponential factor (σ_0) and activation enthalpy (ΔH) of pressure
250 dependence can be illustrated as the relations of $\sigma_0 = A_0(1-BP)$ and $\Delta H = \Delta U + P\Delta V$. All
251 of the listed parameters including ΔU , ΔV , and P stand for the activation energy (eV),
252 the activation volume ($\text{cm}^3 \text{ mole}^{-1}$) and pressure (GPa), and as well as B is representing
253 a constant, respectively. Furthermore, the electrical conductivity of gabbroic melt along
254 with the variations of temperature, pressure and water content is fitted accordingly and
255 the detailed fitting results are displayed in Table 3. The logarithmic electrical
256 conductivity of gabbroic melt with a fixed water content of 2.59 wt% and the inverse
257 temperature follows a good linear relation, which reveals only one main conduction
258 mechanism operating the electrical transport within our experimental temperature and
259 pressure ranges. By virtue of the available pressure-dependent electrical conductivity,



260 we also can extrapolate the relationship between the electrical conductivity of gabbroic
261 melt with a fixed water content of 2.59 wt% and temperature at atmospheric pressure.
262 And then the pre-exponential factor and activation enthalpy at room pressure are
263 calculated as 5177 S m^{-1} and 0.87 eV, respectively. According to Eq. 5 and Table 3, the
264 activation energy and activation volume of gabbroic melt with a fixed water content of
265 2.59 wt% can be determined as $0.87 \pm 0.04 \text{ eV}$ and $-1.98 \pm 0.52 \text{ cm}^3 \text{ mole}^{-1}$.

266 **4.2 Influence of water content on electrical conductivity**

267 For a fixed pressure of 1.0 GPa, the influence of water content on the electrical
268 conductivity of gabbroic melt at temperature range of 873–1373 K is detailedly shown
269 in Fig. 6. The electrical conductivity of gabbroic melt with four different water contents
270 gradually increases with the rise of temperature. For each correspondent water content
271 (i.e. 0, 2.59 wt%, 5.92 wt% and 8.32 wt%), the logarithm of electrical conductivity of
272 the sample and reciprocal temperature follows a good linear relation. On the other hand,
273 when water content of gabbroic melt enhances from 0 to 8.32 wt%, the electrical
274 conductivity of gabbroic melts tends to visibly increase, and whereas the activation
275 enthalpy gradually reduces from 0.93 eV to 0.63 eV, accordingly. In short, our presently
276 acquired electrical conductivity results show a substantial enhancement of water on the
277 electrical conductivity of gabbroic melt, which are also observed among the electrical
278 conductivity of other representative calc-alkaline igneous rock melts in the recent years
279 (Ni et al., 2011; Laumonier et al., 2015; Guo et al., 2017; Chen et al., 2018).

280 The electrical conductivity of hydrous gabbroic melt can be expressed in terms of
281 the charge species concentration dependence of the pre-exponential factor (A), which



282 behaves in an Arrhenius relation,

$$283 \quad \sigma = (A_1 + A_2 \cdot C_w^r) \cdot \exp\left(\frac{-\Delta H_0 - \alpha C_w^\beta}{RT}\right) \quad (6)$$

284 In here, C_w is water content of the sample (wt%), ΔH_0 stands for the activation enthalpy,

285 and α , β and r stand for empirical power-law constants. By a non-linear global least-

286 squares method, the electrical conductivity of gabbroic melt with different water

287 contents was fitted and the fitted parameter results were listed in Table 4. For the

288 magnitude of water-dependent relation of r (0.43 ± 0.05), it makes clear that the water

289 can dramatically enhance the electrical conductivity of gabbroic melt at conditions of

290 873–1373 K and 1.0 GPa.

291 **4.3 Comparisons with previous studies**

292 As displayed in Fig. 7, five previously reported results on the electrical

293 conductivity of natural gabbro samples were employed to compare with our absolutely

294 new results for the electrical conductivity of gabbroic melt (Sato and Ida, 1984;

295 Schilling et al., 1997; Maumus et al., 2005; Dai et al., 2015; Saito and Bagdassarov,

296 2018). As a whole, our acquired electrical conductivity results on gabbroic melts are

297 obviously higher than those of natural gabbro at temperature range of 873–1373 K and

298 pressure of 1.0 GPa. Both Sato and Ida (1984) and Schilling et al. (1997) have already

299 performed the electrical conductivity measurements on natural gabbro at high

300 temperature and atmospheric pressure. In case of the occurrence of temperature-

301 induced partial melting, the electrical conductivity of sample will be increased rapidly

302 by several orders of magnitude. However, we find that there is no any relevant

303 information on the water content for their previously reported electrical conductivity



304 results on those of listed melting-bearing natural gabbro samples. The electrical
305 conductivity results of natural gabbro containing 34 vol% melt from Maumus et al.
306 (2005) are much lower than those of our present gabbroic melt, and the obvious
307 discrepancy is possibly caused from the differentiation of the chemical composition and
308 water content of gabbroic melt. In comparison with Saito and Bagdassarov (2018), there
309 is a jump of three orders of magnitude in the electrical conductivity of sample, which
310 is possibly originated from a relatively larger influence of melt volume percentage. As
311 far as the previously reported electrical conductivity of natural gabbro with a relatively
312 lower water content of ~610 ppm and free of any melt by Dai et al. (2015) at pressures
313 of 0.5–2.0 GPa, there is an approximate electrical conductivity result on the anhydrous
314 gabbroic melt to be observed in the present studies. And however, the dependence of
315 electrical conductivity of anhydrous and hydrous gabbroic melts on the temperature,
316 pressure and water content is still scarce under high-temperature and high-pressure
317 conditions until now.

318 It is well known that the gabbroic melt is belonging to one type of representative
319 calc-alkaline igneous rock. As usual, previously available conductivity results
320 confirmed that the electrical conductivity of calc-alkaline igneous rock melts (i.e.
321 dacitic melt, andesitic melt and basaltic melt) is also highly sensitive to the influential
322 factor of the degree of depolymerization at high temperature and high pressure (Ni et
323 al., 2011; Laumonier et al., 2015; Guo et al., 2017). The degree of depolymerization
324 can be characterized by the ratio of non-bridging oxygen ions per tetrahedrally
325 coordinated cation (NBO/T). As pointed out by Mysen et al. (1982), the magnitude of



326 degree of depolymerization on gabbroic melt can be worked out by our above–
327 mentioned EPMA results in Table 1. And the dependence relation of electrical
328 conductivity of gabbroic melts and degree of depolymerization was clearly displayed
329 in Fig. 8 under conditions of four different water contents (i.e. 0, 2.59 wt%, 5.92 wt%
330 and 8.32 wt%), 1373 K and 1.0 GPa. Under constant degree of depolymerization, it
331 makes clear that a relatively lower electrical conductivity is observed in the anhydrous
332 gabbroic melt under condition of 1373 K and 1.0 GPa. With the rise of water content,
333 the electrical conductivity of gabbroic melts dramatically increases, whereas the
334 variation degree for the electrical conductivity gradually reduces. At the same time, we
335 also compared the presently obtained electrical conductivity results for anhydrous and
336 hydrous gabbroic melts with other three representative calc–alkaline igneous melts
337 reported by Ni et al. (2011), Laumonier et al. (2015) and Guo et al. (2017), as detailedly
338 illustrated in Fig. 8. On the base of the previously calculating method for the degree of
339 depolymerization (NBO/T) of melt transforming the detailed EPMA data, the
340 magnitudes in the degree of depolymerization for our present gabbroic melt and other
341 three representative calc–alkaline igneous rock melts (i.e. dacitic melt, andesitic melt
342 and basaltic melt) are 0.65, 0.07, 0.35 and 0.81, respectively. As a whole, the electrical
343 conductivity of four typical calc–alkaline igneous rock melts will increase with the rise
344 of the degree of depolymerization at a fixed water content. As the water content will be
345 enhanced from 0 to 8.32 wt%, the electrical conductivity of each calc–alkaline igneous
346 rock melts will dramatically increase. It is obviously observed that the correspondent
347 variations in the electrical conductivity of calc–alkaline igneous rock melts along the



348 orders from dacitic melt to andesitic melt to gabbroic melt to basaltic melt tend to
349 gradually reduce, and become more and more convergent, accordingly. To my best
350 knowledge, the magnitude in the degree of depolymerization (NBO/T) for the melt
351 sample is highly positive relation with the content variations of alkali-bearing and alkali
352 earth-bearing cations (i.e. Na^+ , K^+ , Ca^{2+} , Mg^{2+} , etc.) (Mysen et al., 1982; Lee et al.,
353 2003; Di Genova et al., 2015). Just as presented the EPMA results, the total contents of
354 alkali cations and alkali-earth cations are determined as the 11.54 wt% of dacitic melt
355 reported by Guo et al. (2017), the 20.41 wt% of andesitic melt reported by Laumonier
356 et al. (2015), the 30.23 wt% of basaltic melt reported by Ni et al. (2011), and as well as
357 the 25.53 wt% of gabbroic melt in this study. And thus, the degree of depolymerization
358 for the calc-alkaline igneous rock melts along the orders from dacitic melt to andesitic
359 melt to gabbroic melt to basaltic melt will gradually increase, accordingly. On the other
360 hand, previous electrical conductivity results have confirmed that the main charge
361 carriers of the calc-alkaline igneous melts are alkali cations and alkali-earth cations at
362 high temperature and high pressure (Ni et al., 2011; Laumonier et al., 2015; Guo et al.,
363 2017; Chen et al., 2018). And thus, the influence of the degree of depolymerization on
364 the electrical conductivity of melt is possibly caused from the concentration of the alkali
365 cations and alkali-earth cations. Accordingly, the electrical conductivity of calc-
366 alkaline igneous melts will gradually increase with the rise of alkali cations and alkali-
367 earth cations along the orders from dacitic melt to andesitic melt to gabbroic melt to
368 basaltic melt. In sum, as followed the orders from dacitic melt to andesitic melt to
369 gabbroic melt to basaltic melt, it is very reasonable that the electrical conductivity of



370 calc-alkaline igneous melts will be gradually enhanced with the rise of degree of
371 depolymerization (NBO/T) under conditions of 1373 K and 1.0 GPa.

372 **5 Geophysical implications**

373 As a typical active plate geotectonic boundary, previously available
374 magnetotelluric results have already revealed that the phenomenon of high conductivity
375 anomalies is widespread distributed in the region of mid-ocean ridge (Key et al., 2013;
376 Miensoopust et al., 2014). For the representative Mohns ridge of the Arctic Ocean, there
377 widely exist a large number of high conductive layers with their conductivity magnitude
378 within the range of $\sim 0.08\text{--}0.32\text{ S m}^{-1}$ at the correspondent depths from 4 km to 7 km
379 (Johansen et al., 2019). All of these acquired seismic and gravitational survey datasets
380 have confirmed that various volume percentages of gabbroic melt widely outcropped
381 in the Mohns ridge of the Arctic Ocean at the depths of $\sim 4\text{--}11$ km (Géli et al., 1994;
382 Conley and Dunn, 2011). And therefore, the high conductivity anomalies in the Mohns
383 ridge of the Arctic Ocean are possibly correlated with the gabbroic melt at high
384 temperature and high pressure. In conjunction with our presently obtained experimental
385 results on the electrical conductivity of anhydrous and hydrous gabbroic melts at
386 conditions of 873–1373 K and 1.0–3.0 GPa, the typical Hashin–Shtrikman upper bound
387 model and previously available magnetotelluric results, the electrical conductivity of
388 gabbroic melt–olivine system was constructed in detail, as displayed in Fig. 9. All of
389 these influential ingredients including water content and volume percentage were
390 comprehensively considered. During the process of the expansion of mid-ocean ridge
391 caused by the rapid upwelling of asthenosphere mantle, the geothermal distribution



392 exhibited an abnormal behavior in the Mohns ridge of the Arctic Ocean. As pointed out
393 by Johansen et al. (2019), the temperature on the top gabbro layer is approximate to
394 1373 K along the ultraslow-spreading Arctic mid-ocean Mohns ridge region. In
395 addition, the effect of pressure on the electrical conductivity of gabbroic melt is rather
396 feeble, and it can be neglected.

397 The electrical conductivity results of gabbroic melt with four different water
398 contents are selected from our present studies. The electrical conductivity of olivine at
399 1373 K and 1.0 GPa is properly extrapolated from the available experimental data of
400 polycrystalline olivine under conditions of 160 ppm wt water content, 873–1273 K and
401 4.0–10.0 GPa reported by Dai and Karato (2014). On the variation of volume
402 percentage for the gabbroic melt, the electrical conductivity of a gabbroic melt–olivine
403 system (σ_{HS+}) can be expressed as (Hashin and Shtrikman, 1962),

$$404 \quad \sigma_{HS+} = \sigma_{melt} + [(1-X_{melt}) \cdot (\sigma_{olivine} - \sigma_{melt})^{-1} + X_{melt} / (3 \cdot \sigma_{melt})]^{-1} \quad (7)$$

405 In here, the signals of σ_{melt} and $\sigma_{olivine}$ stand for the electrical conductivity of gabbroic
406 melt from the present study and that of polycrystalline olivine with a certain water
407 content of 160 ppm wt from Dai and Karato (2014), respectively; X_{melt} stands for the
408 volume percentage of gabbroic melt.

409 The electrical conductivity of gabbroic melt–olivine system with different volume
410 percentage of gabbroic melt was successfully worked out at 1373 K and 1.0 GPa, as
411 displayed in Fig. 9. For the gabbroic melt–olivine system with a certain volume
412 percentage of gabbroic melt, the electrical conductivity increases with the rise of water
413 content in gabbroic melt. As far as the gabbroic melt containing a fixed water content,



414 the electrical conductivity of gabbroic melt–olivine system gradually enhances as the
415 volume percentage of gabbroic melt increases. As pointed out by Johansen et al. (2019),
416 the range of electrical conductivity for the HCL in the Mohns ridge is $\sim 0.08\text{--}0.32\text{ S m}^{-1}$,
417 as displayed in the orange region of Fig. 9. For the anhydrous gabbroic melt, the
418 required volume percentage for the high conductivity anomalies the ultraslow-
419 spreading Arctic mid-ocean Mohns ridge region falls within the range of $\sim 2.93\text{--}34.69$
420 vol%, which is in good agreement with previously inferred results from geophysical
421 observations (Géli et al., 1994; Conley and Dunn, 2011). When the water content of
422 gabbroic melt increases, the required volume percentage for the HCL reduces
423 accordingly. As for the gabbroic melt with a relatively high water content of 8.32 wt%,
424 its volume percentage range of $\sim 1.32\%\text{--}16.97\text{ vol}\%$ is enough to explain the high
425 conductivity anomalies. In summary, the high conductivity anomalies in the Mohns
426 ridge of the Arctic Ocean could be interpreted by the anhydrous and hydrous gabbroic
427 melt, and our present electrical conductivity results for gabbroic melt with different
428 water contents can provide an important constraint for the water content and volume
429 percentage of gabbroic melt at depth range of $\sim 4\text{--}7\text{ km}$ within the Mohns ridge region
430 of the Arctic Ocean.

431

432 **Conclusions**

433 In the present studies, the electrical conductivity of gabbroic melt with different
434 water contents of 0–8.32 wt% were measured at temperatures of 873–1373 K and
435 pressures of 1.0–3.0 GPa. For the gabbroic melt with a fixed water content of 2.59 wt%,



436 the electrical conductivity of the sample decreases slightly with the rise of pressure, and
437 its corresponding activation energy and activation volume are determined as 0.87 ± 0.04
438 eV and $-1.98 \pm 0.02 \text{ cm}^3 \text{ mole}^{-1}$, respectively. When water content of gabbroic melt
439 enhances from 0 to 8.32 wt% under the certain conditions of 873–1373 K and 1.0 GPa,
440 the electrical conductivity of gabbroic melts tends to visibly increase, and whereas the
441 activation enthalpy gradually reduces from 0.93 eV to 0.63 eV, accordingly.
442 Furthermore, the functional relation models for the electrical conductivity of gabbroic
443 melt with the variations of temperature, pressure and water content are constructed at
444 high-temperature and high-pressure conditions, respectively. By virtue of typical
445 Hashin–Shtrikman upper bound model, the electrical conductivity of gabbroic melt–
446 olivine system on the variation of melt volume percentage is calculated under the
447 conditions of four different water contents of gabbroic melt (i.e. 0, 2.59 wt%, 5.92 wt%
448 and 8.32 wt%), 1373 K and 1.0 GPa, which can be employed to reasonably explain the
449 high conductivity anomalies in the Mohns ridge of the Arctic Ocean observed by the
450 previously available field MT results.

451 *Data availability.* The data that support the findings of this study are available from
452 the first author upon reasonable request.

453 *Acknowledgements.* This research was financially supported by the NSF of China
454 (grant number 42072055 and 42274137) and the Youth Innovation Promotion
455 Association of CAS (grant number 2019390).

456 *Declaration of competing interest.* The authors declare that they have no conflict

<https://doi.org/10.5194/egusphere-2023-345>

Preprint. Discussion started: 21 March 2023

© Author(s) 2023. CC BY 4.0 License.



457 of interest.



458 **References**

- 459 Almeev, R., Holtz, F., Koepke, J., Haase, K., and Devey, C.: Depths of partial
460 crystallization of H₂O-bearing MORB: Phase equilibria simulations of basalts at
461 the MAR near Ascension Island (7–11°S), *J. Petrol.*, 49, 25–45, 2008.
- 462 Chen, J. Y., Gaillard, F., Villaros, A., Yang, X. S., Laumonier, M., Jolivet, L., Unsworth,
463 M., Hashim, L., Scaillet, B., and Richard, G.: Melting conditions in the modern
464 Tibetan crust since the Miocene, *Nat. Commun.*, 9, 3515,
465 <https://doi.org/10.1038/s41467-018-05934-7>, 2018.
- 466 Conley, M. M. and Dunn, R. A.: Seismic shear wave structure of the uppermost mantle
467 beneath the Mohns Ridge, *Geochem. Geophys. Geosyst.*, 12, Q0AK01,
468 <https://doi.org/10.1029/2011GC003792>, 2011.
- 469 Dai, L. D., Li, H. P., Hu, H. Y., and Shan, S. M.: Experimental study of grain boundary
470 electrical conductivities of dry synthetic peridotite under high-temperature, high-
471 pressure, and different oxygen fugacity conditions, *J. Geophys. Res. Solid Earth*,
472 113, B12211, <https://doi.org/10.1029/2008JB005820>, 2008.
- 473 Dai, L. D., Li, H. P., Hu, H. Y., and Shan, S. M.: Novel technique to control oxygen
474 fugacity during high-pressure measurements of grain boundary conductivities of
475 rocks, *Rev. Sci. Instrum.*, 80, 033903, <https://doi.org/10.1063/1.3097882>, 2009.
- 476 Dai, L. D. and Karato, S. I.: The effect of pressure on the electrical conductivity of
477 olivine under the hydrogen-rich conditions, *Phys. Earth and Planet. Inter.*, 232, 51–
478 56, 2014.
- 479 Dai, L. D., Hu, H. Y., Li, H. P., Hui, K. S., Jiang, J. J., Li, J., and Sun, W. Q.: Electrical



- 480 conductivity of gabbro: The effects of temperature, pressure and oxygen fugacity,
481 Eur. J. Mineral., 27, 215–224, 2015.
- 482 Dai, L. D. and Karato, S. I.: Electrical conductivity of Ti-bearing hydrous olivine
483 aggregates at high temperature and high pressure, J. Geophys. Res. Solid Earth,
484 125, e2020JB020309, <https://doi.org/10.1029/2020JB020309>, 2020.
- 485 Di Genova, D., Morgavi, D., Hess, K. U., Neuville, D. R., Borovkov, N., Perugini, D.,
486 and Dingwell, D. B.: Approximate chemical analysis of volcanic glasses using
487 Raman spectroscopy, J. Raman Spectrosc., 46, 1235–1244, 2015.
- 488 Dixon, J. B., Stolper, E. M., and Holloway, J. R.: An experimental study of water and
489 carbon dioxide solubilities in mid-ocean ridge basaltic liquids. Part I: Calibration
490 and solubility models, J. Petrol., 36, 1607–1631, 1995.
- 491 Förster, M. W. and Selway, K.: Melting of subducted sediments reconciles geophysical
492 images of subduction zones, Nat. Commun., 12, 1320,
493 <https://doi.org/10.1038/s41467-021-21657-8>, 2021.
- 494 Géli, L., Renard, V., and Rommevaux, C.: Ocean crust formation processes at very slow
495 spreading centers: A model for the Mohns Ridge, near 72°N, based on magnetic,
496 gravity, and seismic data, J. Geophys. Res. Solid Earth, 99, 2995–3013, 1994.
- 497 Guo, X., Li, B., Ni, H. W., and Mao, Z.: Electrical conductivity of hydrous andesitic
498 melts pertinent to subduction zones, J. Geophys. Res. Solid Earth, 122, 1777–1788,
499 2017.
- 500 Hashin, Z. and Shtrikman, S.: A variation approach to the theory of effective magnetic
501 permeability of multiphase materials, J. Appl. Phys., 33, 3125–3131, 1962.



- 502 Hong, M. L., Dai, L. D., Hu, H. Y., Yang, L. F. and Zhang, X. Y.: Pressure-induced
503 structural phase transitions in natural kaolinite investigated by Raman
504 spectroscopy and electrical conductivity, *Am. Mineral.*, 107, 385–394, 2022.
- 505 Hu, H. Y., Dai, L. D., Sun, W. Q., Wang, M. Q., and Jing, C. X.: Constraints on fluids
506 in the continental crust from laboratory-based electrical conductivity
507 measurements of plagioclase, *Gondwana Res.*, 107, 1–12, 2022a.
- 508 Hu, H. Y., Jing, C. X., Dai, L. D., Yin, C. Y. and Chen, D. M.: Electrical conductivity
509 of siderite and its implication for high conductivity anomaly in the slab-mantle
510 wedge interface, *Front. Earth Sci.*, 10, 985740,
511 <https://doi.org/10.3389/feart.2022.985740>, 2022b.
- 512 Huebner, J. S. and Dillenburg, R. G.: Impedance spectra of hot, dry silicate minerals
513 and rock: Qualitative interpretation of spectra, *Am. Mineral.*, 80, 46–64, 1995.
- 514 Johansen, S. E., Panzner, M., Mittet, R., Amundsen, H. E. F., Lim, I., Vik, E., Landrø,
515 M., and Arntsen, B.: Deep electrical imaging of the ultraslow-spreading Mohns
516 ridge, *Nature*, 567, 379–383, 2019.
- 517 Key, K., Constable, S., Liu, L. J., and Pommier, A.: Electrical image of passive mantle
518 upwelling beneath the northern East Pacific Rise, *Nature*, 495, 499–502, 2013.
- 519 Laumonier, M., Gaillard, F., and Sifre, D.: The effect of pressure and water
520 concentration on the electrical conductivity of dacitic melts: Implication for
521 magnetotelluric imaging in subduction areas, *Chem. Geol.*, 418, 66–76, 2015.
- 522 Lee, S. K., Mysen, B. O., and Cody, G. D.: Chemical order in mixed-cation silicate
523 glasses and melts, *Phys. Rev. B*, 68, 214206,



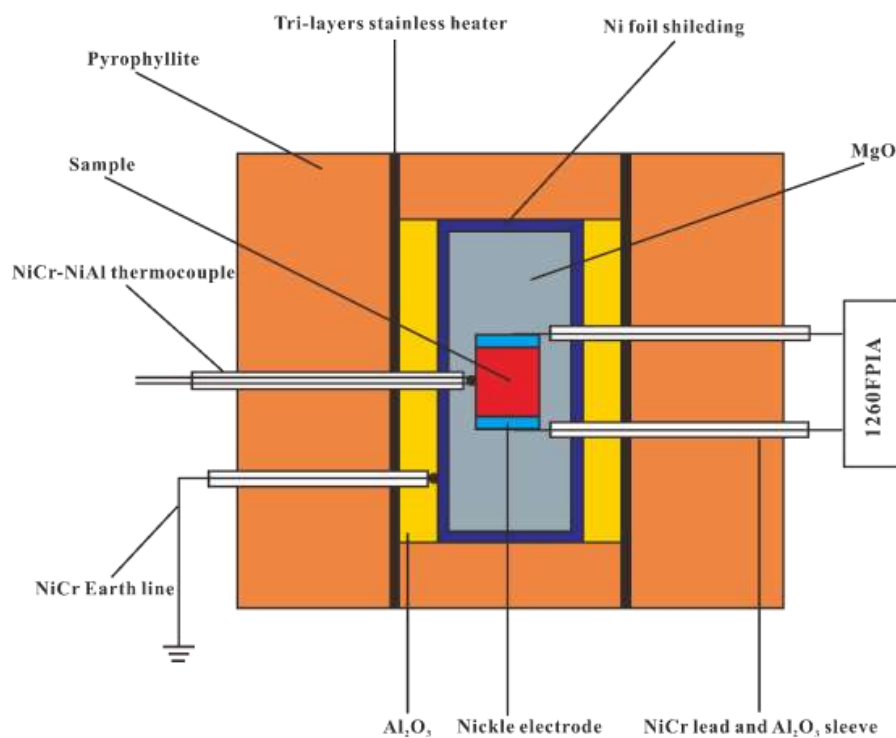
- 524 <https://doi.org/10.1103/PhysRevB.68.214206>, 2003.
- 525 Leuthold, J., Lissenberg, C. J., O'Driscoll, B., Karakas, O., Falloon, T., Klimentyeva,
526 D. N., and Ulmer, P.: Partial melting of lower oceanic crust gabbro: Constraints
527 from poikilitic clinopyroxene primocrysts, *Front. Earth Sci.*, 6, 15,
528 <https://doi.org/10.3389/feart.2018.00015>, 2018.
- 529 Li, G. H., Gao, Y., Zhou, Y. Z., Ju, C. H., Shi, Y. T., and Cui, Q. H.: A low-velocity
530 layer atop the mantle transition zone beneath the western Central Asian Orogenic
531 Belt: Upper mantle melting induced by ancient slab subduction, *Earth Planet. Sci.*
532 *Let.*, 578, 117287, <https://doi.org/10.1016/j.epsl.2021.117287>, 2022.
- 533 Luhr, J. F.: Glass inclusions and melt volatile contents at Parícutin Volcano, Mexico,
534 *Contrib. Mineral. Petrol.*, 142, 261–283, 2001.
- 535 Maumus, J., Bagdassarov, N., and Schmeling, H.: Electrical conductivity and partial
536 melting of mafic rocks under pressure, *Geochim. Cosmochim. Ac.*, 69, 4703–4718,
537 2005.
- 538 Miensoyust, M. P., Jones, A. G., Hersir, G. P., and Vilhjálmsson, A. M.: The
539 Eyjafjallajökull volcanic system, Iceland: Insights from electromagnetic
540 measurements, *Geophys. J. Int.*, 199, 1187–1204, 2014.
- 541 Mysen, B. O., Virgo, D., and Seifert, F. A.: The structure of silicate melts: Implications
542 for chemical and physical properties of natural magma, *Rev. Geophys.*, 20, 353–
543 383, 1982.
- 544 Ni, H. W., Keppler, H., and Behrens, H.: Electrical conductivity of hydrous basaltic
545 melts: Implications for partial melting in the upper mantle, *Contrib. Mineral.*



- 546 Petrol., 162, 637–650, 2011.
- 547 Saito, S. and Bagdassarov, N. S.: Laboratory measurements of electrical conductivity in
548 a gabbro of the Oman ophiolite at high–pressures and high–temperatures:
549 Implications for interpretation of resistivity structures of lower oceanic crust, J.
550 Mineral. Petrol. Sci., 113, 112–117, 2018.
- 551 Salta, V., Vallianatos, F., and Gidarakos, E.: Charge transport in diatomaceous earth
552 studied by broadband dielectric spectroscopy, Appl. Clay Sci., 80–81, 226–235,
553 2013.
- 554 Salta, V., Pentari, D., and Vallianatos, F.: Complex electrical conductivity of biotite and
555 muscovite micas at elevated temperatures: A comparative study, Materials, 13,
556 3513, <https://doi.org/10.3390/ma13163513>, 2020.
- 557 Sato, H. and Ida, Y.: Low frequency electrical impedance of partially molten gabbro:
558 the effect of melt geometry on electrical properties, Tectonophysics, 107, 105–134,
559 1984.
- 560 Schilling, F. R., Partzsch, G. M., Brasse, H., and Schwarz, G.: Partial melting below the
561 magmatic arc in the central Andes deduced from geoelectromagnetic field
562 experiments and laboratory data, Phys. Earth Planet. In., 103, 17–31, 1997.
- 563 Shaw, A. M., Behn, M. D., Humphris, S. E., Sohn, R. A., and Gregg, P. M.: Deep
564 pooling of low degree melts and volatile fluxes at the 85°E segment of the Gakkel
565 Ridge: Evidence from olivine-hosted melt inclusions and glasses, Earth Planet. Sci.
566 Lett., 289, 311–322, 2010.
- 567 Shen, Y. and Forsyth, D. W.: Geochemical constraints on initial and final depths of

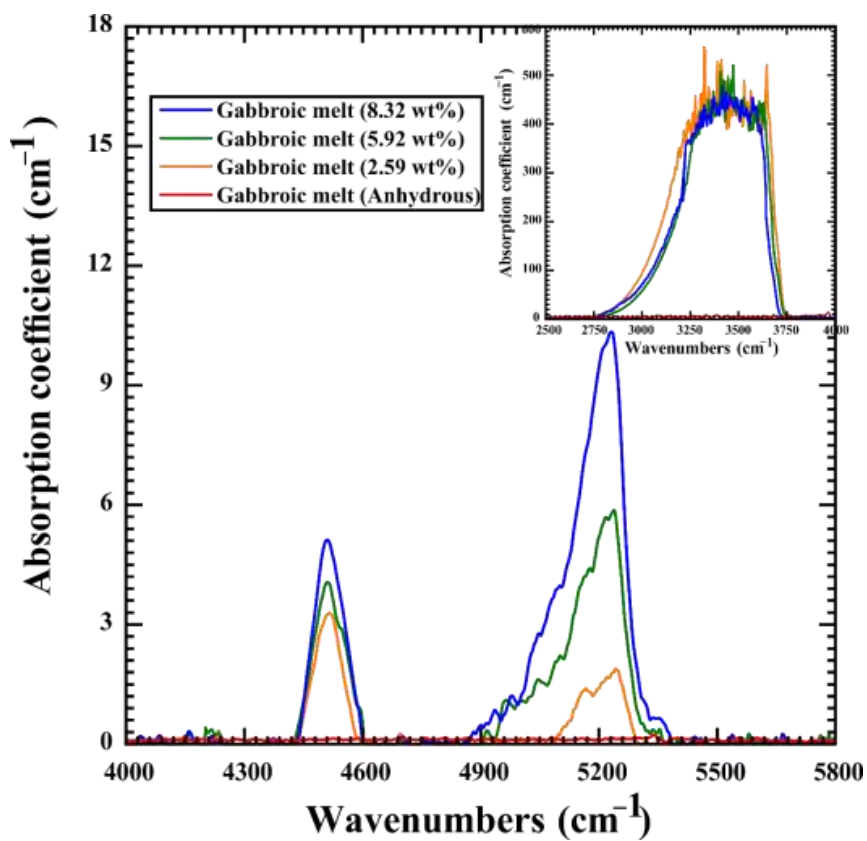


- 568 melting beneath mid-ocean ridges, *J. Geophys. Res. Solid Earth*, 100, 2211–2237,
569 1995.
- 570 Sim, S. J., Spiegelman, M., Stegman, D. R., and Wilson, C.: The influence of spreading
571 rate and permeability on melt focusing beneath mid-ocean ridges, *Phys. Earth
572 Planet. Inter.*, 304, 106486, <https://doi.org/10.1016/j.pepi.2020.106486>, 2020.
- 573 Stolper, E.: The speciation of water in silicate melts, *Geochim. Cosmochim. Ac.*, 46,
574 2609–2620, 1982.
- 575 Turner, S. J. and Langmuir, C. H.: Sediment and ocean crust both melt at subduction
576 zones, *Earth Planet. Sci. Lett.*, 584, 117424,
577 <https://doi.org/10.1016/j.epsl.2022.117424>, 2022.
- 578 Wallace, P. J.: Volatiles in subduction zone magmas: concentrations and fluxes based
579 on melt inclusion and volcanic gas data, *J. Volcanol. Geoth. Res.*, 140, 217–240,
580 2005.
- 581 White, R. S., Minshull, T.A., Bickle, M. J., and Robinson, C. J.: Melt generation at very
582 slow-spreading oceanic ridges: Constraints from geochemical and geophysical
583 data, *J. Petrol.*, 42, 1171–1196, 2001.
- 584 Wu, K., Ling, M. X., Hu, Y. B., Guo, J., Jiang, X. Y., Sun, S. J., Liang, H. Y., Liu, X.,
585 and Sun, W. D.: Melt-fluxed melting of the heterogeneously mixed lower arc crust:
586 A case study from the Qinling orogenic belt, Central China, *Geochem. Geophys.
587 Geosyst.*, 19, 1767–1788, 2018.
- 588 Xu, Y. S., Shankland, T. J., and Duba, A. G.: Pressure effect on electrical conductivity
589 of mantle olivine, *Phys. Earth Planet. Inter.*, 118, 149–161, 2000.



590

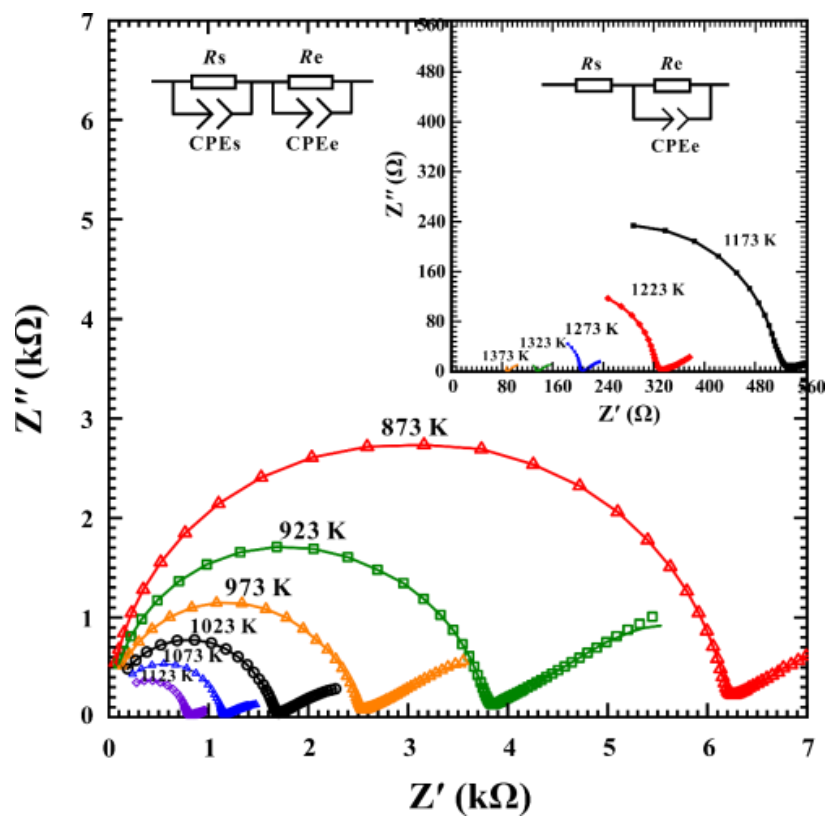
591 **Figure 1.** The experimental setup for the electrical conductivity measurements of
592 gabbroic melt at high temperatures and high pressures.



593

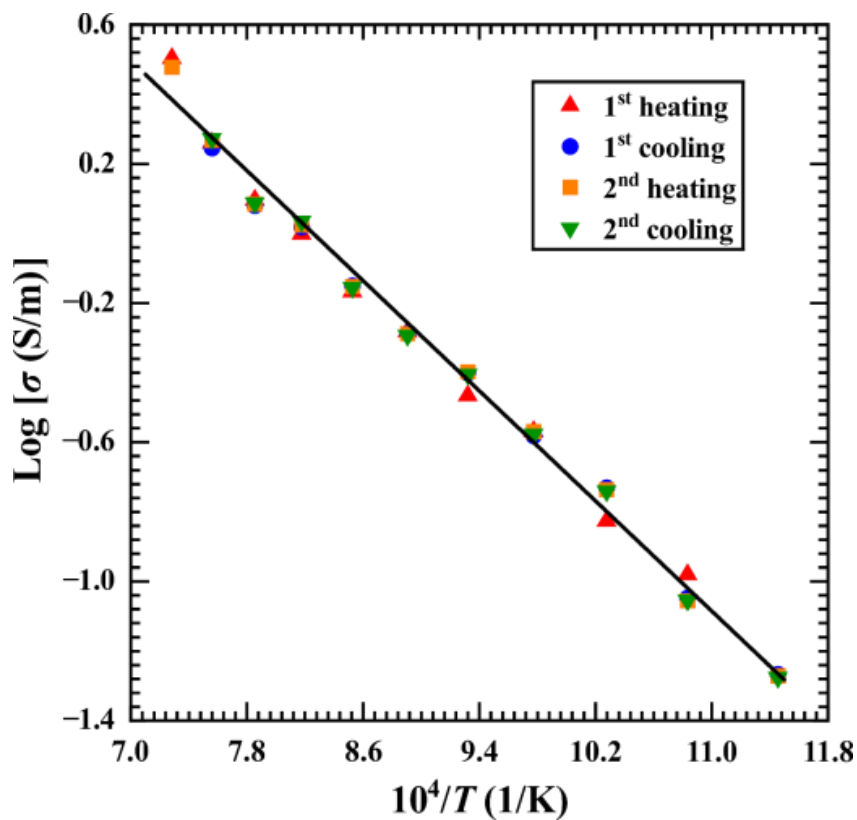
594 **Figure 2.** The representative FT-IR spectra of the gabbroic melt with various water

595 contents in the wavenumbers range of 4000–5800 cm^{-1} and 2500–4000 cm^{-1} .



596

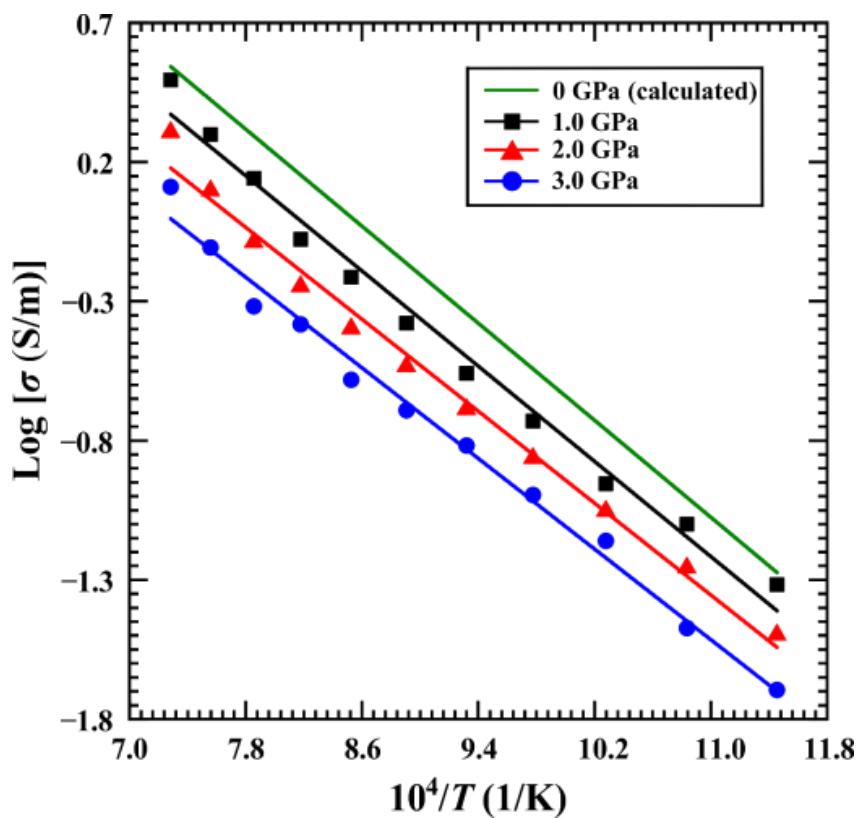
597 **Figure 3.** Typical complex impedance spectra for gabbroic melt with a fixed water
598 content of 2.59 wt% (DW209) at temperatures of 873–1373 K and pressure of 2.0 GPa
599 in the frequency range from 10^0 Hz to 10^6 Hz. The fitting results for the experimental
600 data are displayed by using the solid line.



601

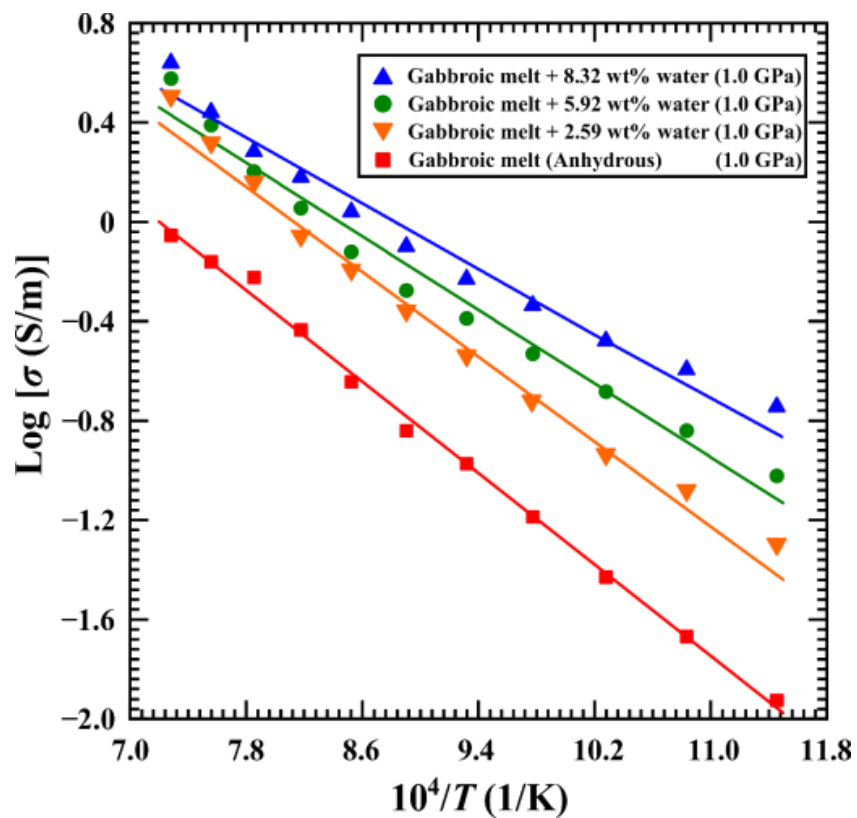
602 **Figure 4.** The electrical conductivity of gabbroic melt with a fixed water content of

603 2.59 wt% (DW212) among two heating-cooling cycles at a pressure of 3.0 GPa.



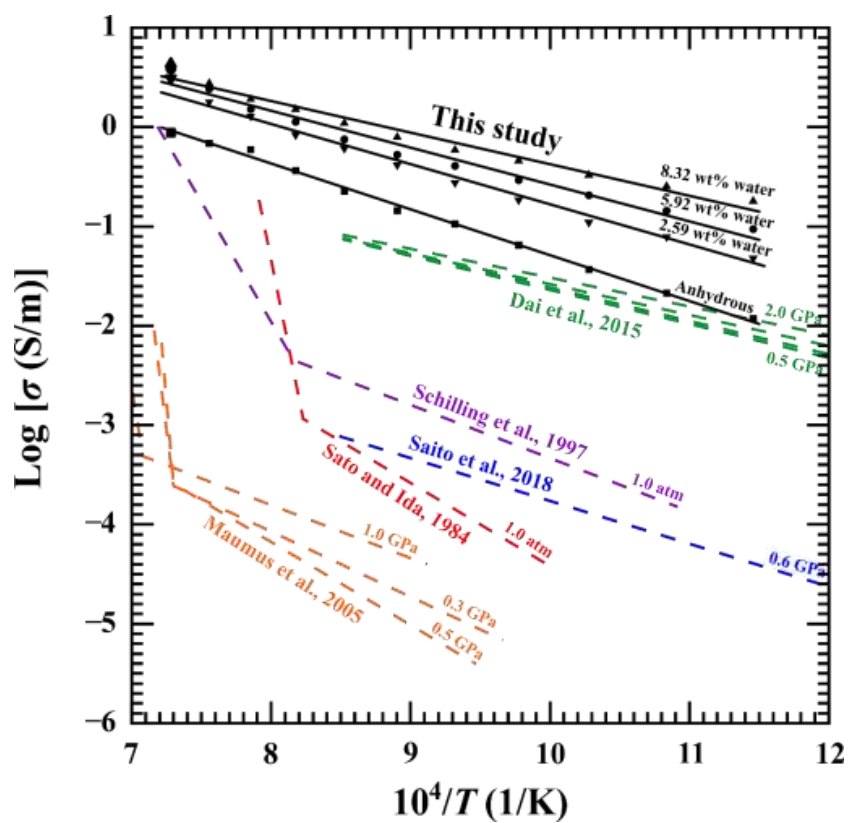
604

605 **Figure 5.** Influence of pressure on the electrical conductivity of gabbroic melt with a
606 fixed water content of 2.59 wt% at the temperature ranges of 873–1373 K.



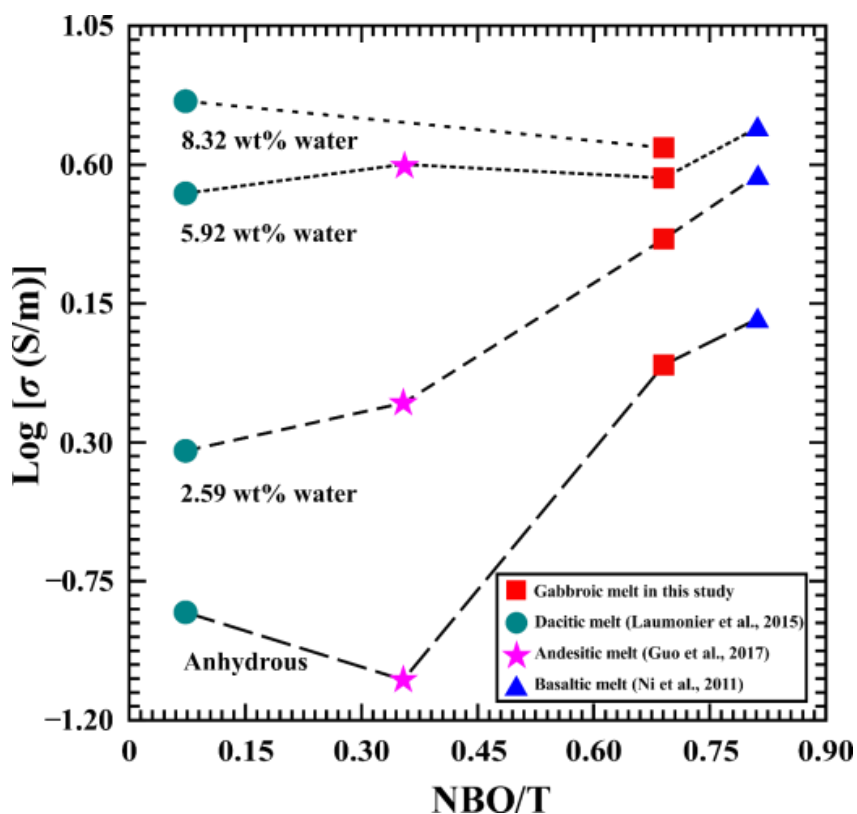
607

608 **Figure 6.** Logarithmic electrical conductivity of gabbroic melts with four different
609 water contents as a function of reciprocal temperature at conditions of 873–1373 K and
610 1.0 GPa.



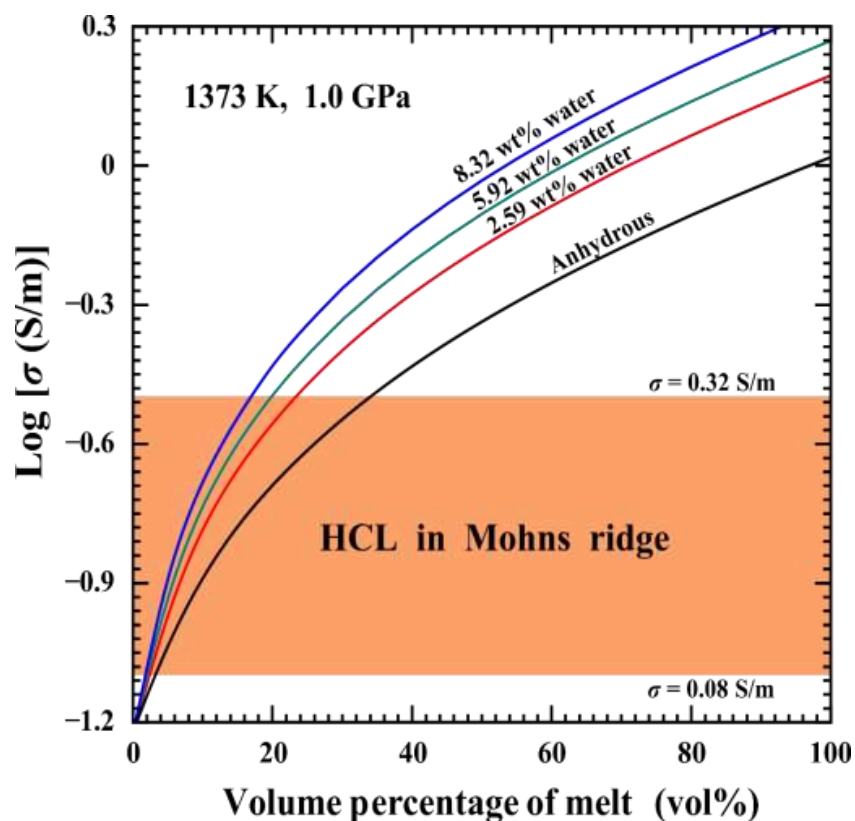
611

612 **Figure 7.** Comparison of electrical conductivity of gabbroic melts with the previously
613 reported results from five natural gabbro samples at high-temperature and high-
614 pressure conditions.



615

616 **Figure 8.** Variation of electrical conductivity of gabbroic melt and three representative
 617 calc-alkaline igneous rock melts with the degree of depolymerization (NBO/T) under
 618 conditions of four different water contents (i.e. 0, 2.59 wt%, 5.92 wt% and 8.32 wt%),
 619 1373 K and 1.0 GPa. Data source: basaltic melt from Ni et al. (2011), andesitic melt
 620 from Guo et al. (2017), and dacitic melt from Laumonier et al. (2015).



621

622 **Figure 9.** The electrical conductivity for the gabbroic melt–olivine system at
 623 temperature of 1373 K and 1.0 GPa, calculated with Eq. 7 of the Hashin–Shtrikman
 624 upper bound model. The electrical conductivity of olivine from Dai and Karato (2014)
 625 was adopted as σ_{olivine} . The orange region indicates the gabbro layer within the electrical
 626 conductivity range of 0.08–0.32 S m⁻¹ along the ultraslow–spreading Arctic mid–ocean
 627 Mohns ridge region (Johansen et al., 2019).



628 **Table 1.** The chemical composition of the gabbroic melts by virtue of the electronic
629 probe microscopy analysis (EPMA).

Sample	SiO ₂	TiO ₂	Al ₂ O ₃	FeO	MnO	MgO	CaO	Na ₂ O	K ₂ O	Total (wt%)
Gabbroic melt (anhydrous)	51.32	0.56	12.37	9.93	0.20	11.06	11.82	2.15	0.50	99.91
Gabbroic melt (2.59 wt% water)	51.22	0.55	12.40	9.92	0.18	11.29	11.72	2.19	0.48	99.95
Gabbroic melt (5.92 wt% water)	51.23	0.57	12.40	9.87	0.18	11.28	11.70	2.21	0.47	99.91
Gabbroic melt (8.32 wt% water)	51.22	0.57	12.40	9.88	0.17	11.27	11.69	2.21	0.46	99.86

630



631 **Table 2.** Fitted parameters of Arrhenius relation for the electrical conductivity of
632 hydrous and anhydrous gabbroic melts under conditions of 873–1373 K and 1.0–3.0
633 GPa.

Sample	T (K)	P (GPa)	Water content Before experiment (wt%)	Water content After experiment (wt%)	$\text{Log } \sigma_0$ (σ_0 in S m^{-1})	ΔH (eV)
DW201	873–1373	1.0	8.32	8.30	2.80 ± 0.16	0.63 ± 0.03
DW204	873–1373	1.0	5.92	5.90	3.13 ± 0.18	0.74 ± 0.04
DW208	873–1373	1.0	2.59	2.57	3.48 ± 0.15	0.85 ± 0.03
DW209	873–1373	2.0	2.59	2.58	3.18 ± 0.13	0.83 ± 0.03
DW212	873–1373	3.0	2.59	2.50	2.79 ± 0.11	0.81 ± 0.03
DW210	873–1373	1.0	0	0	3.31 ± 0.08	0.93 ± 0.02

634



635 **Table 3.** Parameter values for the electrical conductivity of gabbroic melt with water
636 content of 2.59 wt% at pressures of 1.0–3.0 GPa. The equation $\sigma = \sigma_0 \cdot \exp\left(-\frac{\Delta U + P\Delta V}{kT}\right)$
637 is adopted for the globally fitting of electrical conductivity data. In consideration of a
638 strong dependence of the pre-exponential factor (σ_0) on the pressure, we used the
639 relation $\sigma_0 = A_0 \cdot (1 - BP)$.

σ_0 (S m ⁻¹)	B (GPa ⁻¹)	ΔU (eV)	ΔV (cm ³ mole ⁻¹)
$A_0 = 2623.27 \pm 1.41$	$B = 0.22 \pm 0.03$	0.87 ± 0.04	-1.98 ± 0.52

640



641 **Table 4.** Parameter values for the electrical conductivity of gabbroic melts with
642 different water contents under conditions of 873–1373 K and 1.0 GPa. The
643 equation $\sigma = (A_1 + A_2 \cdot C_w^r) \cdot \exp\left(\frac{-\Delta H_0 - \alpha C_w^\beta}{RT}\right)$ is adopted for the globally fitting of electrical
644 conductivity data.

A_1 (S m ⁻¹)	A_2 (S m ⁻¹)	ΔH_0 (eV)	α	β	r
6760±234	66069±240	1.03±0.04	34.85±2.24	17.70±1.31	0.43±0.05

645